Research Article Vol. 32, No. 14 / 1 Jul 2024 / Optics Express 24081
Optics EXPRESS

Low loss polycrystalline SiGe core fibers for nonlinear photonics

AMAR N. GHOSH,[1,*] MENG HUANG,[1] THOMAS W. HAWKINS,[2] JOHN BALLATO,[2] URSULA J. GIBSON,[3] AND ANNA C. PEACOCK[1]

[1]Optoelectronics Research Center, University of Southampton, Southampton, SO17 1BJ, UK
[2]Center for Optical Materials Science and Engineering Technologies and Department of Materials Science and Engineering, Clemson University, Clemson, SC 29634, USA
[3]Dartmouth Thayer School of Engineering, Hanover, NH 03755, USA
[*]A.N.Ghosh@soton.ac.uk

Abstract: Polycrystalline silicon-germanium (SiGe) core fibers offer great potential as flexible platforms for microscale optoelectronic and nonlinear optical devices. Compared to silicon (Si) core fibers, the SiGe material provides the potential for higher nonlinear coefficients, extended mid-infrared wavelength coverage, and a means to tune the bandgap and index of refraction by varying the Ge composition. Here, SiGe core fibers (10 at% Ge) were fabricated using the molten core drawing method, followed by CO_2 laser irradiation to improve the homogeneity of the core. The transmission properties of the fibers were further optimized using a fiber tapering method to tailor the core diameter and re-grow the crystal grains. The resulting tapered SiGe fiber exhibited an average linear loss of $\sim 3\,\mathrm{dB\,cm^{-1}}$ across the wavelength range $1.5 - 2.5$ μm, allowing for nonlinear optical characterization of this new fiber type. Measurements of the nonlinear figure of merit demonstrate the potential for higher nonlinear performance compared to the pure Si core fibers, particularly for wavelengths >2 μm, indicating that the SiGe fiber platform could open up new opportunities for mid-infrared nonlinear photonics.

1. Introduction

Over the past decade, silicon (Si) core fibers have emerged as a useful platform for nonlinear photonics [1–3]. Through optimization of the fabrication processes, these fibers can now be produced with core dimensions ranging from a few microns down to hundreds of nanometers, with transmission losses that are comparable to, or even less than those for conventional planar silicon waveguides [4,5,7]. This has allowed for the demonstration of a wide range of nonlinear effects including parametric amplification [6], stimulated Raman scattering [7] and supercontinuum generation [5], spanning the telecom band up to the mid-infrared. Interestingly, although other semiconductor core fibers have been fabricated that offer access to different transmission windows and nonlinear parameters, including those incorporating germanium [8], zinc selenide [9], and gallium arsenide [10], in general the transmission losses of these alternative core materials have been too large to observe nonlinear propagation.

An alternative approach that allows for the adjustment of the nonlinearity and wavelength coverage of the semiconductor fibers is to combine other elements such as germanium, within the Si core during the fabrication. Importantly, such fibers can still be made using the optimised Si core fiber fabrication procedures, whilst tuning the composition of the SiGe alloy provides a route to tailor the bandgap and index of refraction [11]. A theoretical investigation of the nonlinear optical coefficients of the SiGe alloy with different germanium concentrations has been previously reported covering the $1 - 10$ μm wavelength range in [12], predicting an increase in the nonlinear

#525754 https://doi.org/10.1364/OE.525754
Journal © 2024 Received 23 Apr 2024; revised 3 Jun 2024; accepted 4 Jun 2024; published 17 Jun 2024

Optics EXPRESS

strength for the entire region compared to pure silicon. However, owing to the strong absorption of germanium for wavelengths below 2 μm, there is a trade off as to how much germanium can be included before the increased propagation loss outweighs any increase in the nonlinearity across the near-infrared region. In this regard, experimental characterization of the nonlinear properties of SiGe waveguides have primarily been limited to selected wavelength bands, either in the telecom region [13], or beyond 3 μm [14], leaving a substantial gap. Moreover, the nonlinear optical properties of the SiGe alloy have yet to be experimentally explored in the fiber platform owing to the relatively high losses reported in the SiGe fibers to-date [11].

In this paper, we investigate the linear and nonlinear transmission properties of polycrystalline SiGe core fibers across the wavelength range spanning 1.5 – 2.5 μm. SiGe fibers (10 at% Ge) with uniform and high crystallinity were fabricated and optimized through several steps, including molten core drawing, CO_2 laser irradiation, and fiber tapering. The relatively low propagation losses that vary from 2.2 dB cm^{-1} at 1.5 μm to 4 dB cm^{-1} at 2.5 μm have allowed for the first characterization of the third-order nonlinear optical coefficients of the SiGe fibers, revealing an enhancement over the Si core fibers, particularly for wavelengths >2 μm. Thus these results highlight the potential for the SiGe fibers to find use in the development of mid-infrared nonlinear fiber systems where applications include sensing, imaging, and spectroscopy.

2. Fabrication of SiGe fibers and tapers

SiGe core fibers with 10 at% Ge concentration were fabricated with a conventional silica cladding using the molten core drawing (MCD) method (see Fig. 1(a)), as described in [11,15]. A calcium oxide (CaO) interface layer was solution cast onto the inner wall of the silica cladding tube as a stress buffer and to prevent oxygen diffusion from the silica cladding into the predominantly Si core. Ge and Si powder were mixed and added into the silica tube after one end had been closed off. This assembly was fed into the hot zone of the draw furnace to pre-melt the powders at 1550 ° C. The assembly was then drawn at 1950 ° C directly into fiber with a core diameter of 35 μm and an outer diameter of 455 μm. The as-drawn SiGe fiber cores are polycrystalline in nature, with longitudinal crystal grain sizes in the range of 0.2 – 1 mm, with electron backscattered diffraction measurements revealing an absence of transverse grain boundaries in the core [11]. To enable optical transmission through the fibers, compositional homogeneity of the SiGe alloy core is required, which is achieved by a CO_2 laser-induced recrystallization process as shown in Fig. 1(b). Although the CO_2 laser processing was only done from one side, the small fiber diameter resulted in a minimal temperature gradient across the sample, as evidenced by the edges of the melt zone being perpendicular to the fiber axis. Rapid cooling due to a graphite heat sink helped to prevent segregation of the constituents and ensure a uniform distribution. Figure 1(c) shows the X-ray computed tomography (XCT) images of the as-drawn and laser-processed fiber core, demonstrating the compositional homogeneity in the fiber after recrystallization. The effect of the recrystallization process has been discussed in detail in [11], where a reduction in the optical transmission loss at 1.55 μm was reported from >20 dB cm^{-1} to 12 dB cm^{-1} following laser processing of a 6 at% Ge concentration fiber. However, the losses and the core diameters of these fibers are still too large to support nonlinear propagation. Thus, in this work we apply an adapted fiber tapering approach as a final post-processing step, similar to what we have developed for the Si core fibers [7,16]. For this purpose, a Vytran tapering rig (GPX-3400) has been used to heat and stretch the SiGe fiber in three steps (see Fig. 1(d)) to reduce the core diameter from 35 μm to 3 μm (in steps of 35 μm → 10.9 μm → 5.2 μm → 3 μm), while at the same time improving the crystallinity and the loss. The final tapered fiber used for the optical characterization had a tapered waist length of 6 cm. Optical microscope images of the final tapered fiber are shown in Figs. 1(e) & (f) where longitudinal view (taken in transmission mode) shows the SiGe core as black and the cross-section (taken in reflective mode) shows it as a bright reflective spot.

Optics EXPRESS

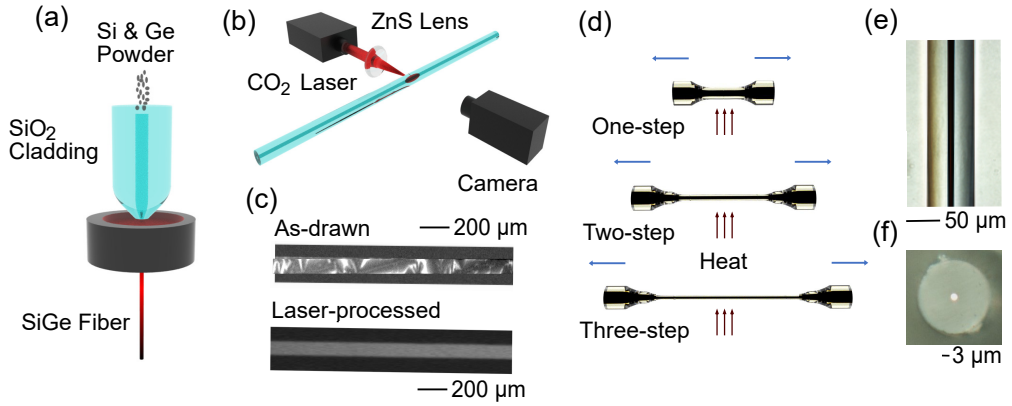

Fig. 1. Fabrication and processing of SiGe fiber. (a) A schematic of the molten core drawing method for fabrication of SiGe fiber. (b) A schematic of the laser recrystallization setup. (c) XCT images of as-drawn and laser-processed fiber. (d) A schematic of the three-step tapering method for fiber optimization. (e) An optical microscope image (taken in transmission mode) of the tapered SiGe fiber, where the SiGe core (black) is clearly visible. (f) Cross-section optical microscope image (taken in reflective mode) of the SiGe fiber with a core diameter of 3 μm.

3. Material characterization

A Raman spectrometer (Renishaw inVia) was used to investigate the improvements to the crystalline quality due to the tapering process. A 532 nm Nd:YAG laser was focused to a spot diameter of 1 μm on the fiber sample using a 50× microscope objective (NA= 0.75) and the measurement was taken by collecting Raman photons using a silicon diffraction grating of 2400 lines/mm with a precision of 0.12 cm^{-1}. Figure 2(a) shows the measured normalized Raman spectra of the SiGe fiber before tapering (black), after the first taper step (red), and after the second taper step (blue). The untapered SiGe fiber shows a polycrystalline silicon Raman peak (Si-Si peak) centered at 510.2 cm^{-1} and two broad Si-Ge peaks centred at 399.3 cm^{-1} and 430.4 cm^{-1}. Here the Si-Si peak is shifted to the left from the characteristic Raman peak of crystalline Si centered at 520 cm^{-1} due to tensile strain present in the fiber [11,17]. Comparing the various spectra, the Si-Ge peaks after the second taper step appear better defined than the peaks of the untapered fiber (see inset of Fig. 2(a)), which indicates a slight improvement of the crystalline quality. However, the material improvement is much more obvious when comparing the stronger Si-Si peak, where there is a clear trend of decreasing linewidth for subsequent tapering procedures, starting from $\Gamma = 3.62 \pm 0.1\ cm^{-1}$ in the untapered SiGe fiber to $3.42 \pm 0.1\ cm^{-1}$ in the one-step tapered SiGe fiber, and down to $3.39 \pm 0.1\ cm^{-1}$ in the two-step tapered fiber, as shown in Fig. 2(b). We attribute this reduction in the linewidth to an increase in the grain size, as has been measured in the Si core fibers [16], indicating an improvement in the polycrystalline quality of the core. We note that the fiber was not measured after the third taper step as it was mounted inside an additional capillary, but we do not expect much change in the linewidth over the second taper step as this is already starting to converge. Furthermore, both the Raman peak position and the linewidth remained remarkably consistent when scanned along the fiber length (variations much less than 1%), confirming the uniformity of the crystallinity within the tapered section.

Optics EXPRESS

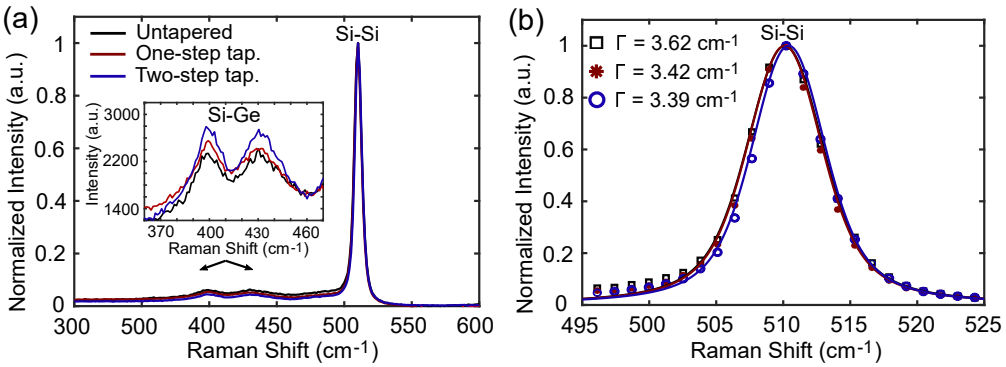

Fig. 2. Material characterization of the SiGe fibers using Raman spectroscopy. (a) The black, red, and blue curves represent the Raman spectra of untapered, one-step tapered, and two-step tapered SiGe fibers, respectively (Inset: Comparison of Si-Ge peaks between untapered, one-step tapered, and two-step tapered SiGe fibers). (b) Comparison of the Si-Si Raman peaks between untapered (black), first-step tapered (red), and second-step tapered (blue) SiGe fibers.

4. Optical transmission properties

In order to explore the optical properties of the tapered SiGe fiber, transmission measurements were performed using the experimental setup shown in Fig. 3(a). An external cavity CW laser (TUNICS, 20 mW (max)) tunable from 1.5 – 1.68 μm and a Cr^{2+}:ZnS/Se laser (IPG Photonics, 3 W (max)) tunable from 2.0 – 2.5 μm were used to probe the linear losses across a wavelength region covering 1.5 – 2.5 μm. The nonlinear parameters were also measured across a similar wavelength region, first using a pulsed fiber laser (Onefive ORIGAMI, 800 fs, 40 MHz, 50 mW (max)) operating at 1.54 μm and then a Yb Oscillator (FLINT) pumped optical parametric oscillator (APE OPO, 250 – 300 fs, 75 MHz, 3 W (max)) across a range of 1.6 – 2.4 μm. The various sources were coupled into the tapered SiGe fiber using a 40× microscope objective (L1) (NA = 0.65) with an average input coupling loss of ~ 4.5 dB over the entire wavelength region and the output light from the fiber was collected and collimated using another 40× microscope objective (L2). CCD cameras (CCD1 & CCD2) were used to aid the optical coupling into and out of the fiber core and ensure that the light was predominantly coupled into the fundamental mode. The input laser power was controlled via a variable neutral density filter and the transmitted light at the fiber output was measured either using a set of power meters (Thorlabs S132C & S148C) or with an optical spectrum analyzer (OSA: Yokagawa AQ 6375) using a final 25× microscope objective (L3) (NA = 0.45).

The refractive index of SiGe alloys with 10 at% Ge is not well documented. Therefore, it was modeled by inserting the standard refractive index of crystalline Si into the formula for $Si_{1-x}Ge_x$, given as $n_{SiGe} \approx n_{Si} + 0.37x + 0.22x^2$ [18,19]. Using the estimated wavelength dependent index, modal analysis was used to calculate the group velocity dispersion parameter (β_2) for the fundamental mode of our 3 μm diameter SiGe fiber, as shown in Fig. 3(b). The fiber exhibits normal dispersion up to the zero dispersion wavelength of 2.78 μm, thanks to the large normal material dispersion of the high index SiGe core. Therefore, any nonlinear characterization in this wavelength region will mainly be driven by self-phase modulation (SPM), and contributions from higher order dispersion can be neglected for pulse propagation and spectral broadening.

Optics EXPRESS

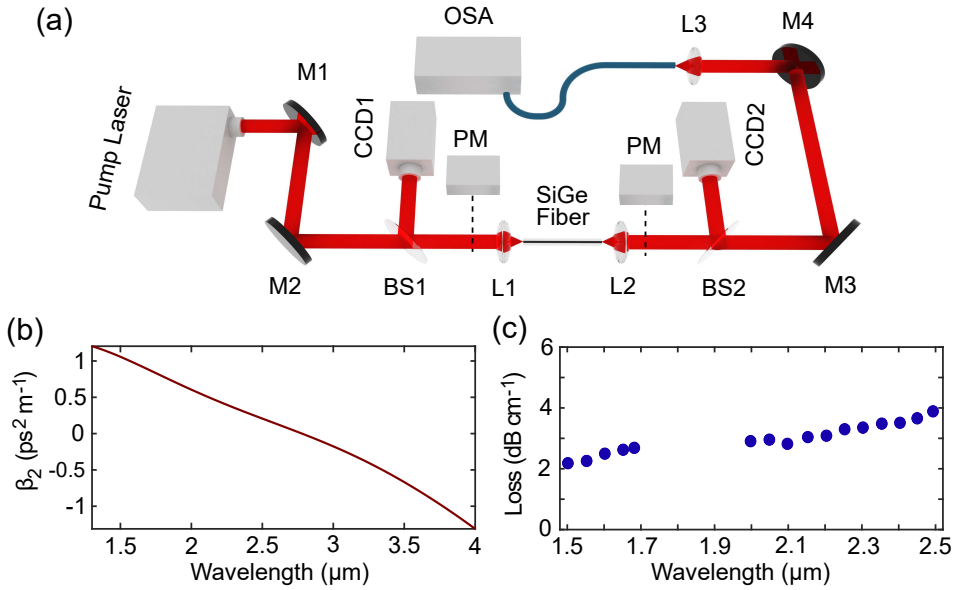

Fig. 3. (a) Schematic of the experimental setup for the optical transmission measurements. Mirrors (M1, M2, M3, & M4), beam-splitters (BS1 & BS2), microscope objective lenses (L1, L2 & L3), CCD Cameras (CCD1 & CCD2), power meters (PM), and optical spectrum analyser (OSA). (b) Calculated dispersion profile for the 3 μm diameter SiGe fiber as a function of wavelength, showing the zero dispersion wavelength located ~ 2.78 μm. (c) Linear propagation losses of the tapered SiGe fiber as a function of wavelength.

4.1. *Linear propagation loss*

Evaluation of the linear propagation loss in the tapered SiGe fiber was carried out using the cut-back method by measuring the total losses within different fiber lengths under a constant light injection condition [20]. Typical values for the losses of the as-drawn and laser processed SiGe fibers are >12 dB cm^{-1} [11]. The results of the loss measurements for the tapered SiGe fiber are plotted in Fig. 3(c), where it can be seen that the losses are much decreased, starting around 2.2 dB cm^{-1} at 1.5 μm before increasing slightly to 4 dB cm^{-1} at 2.5 μm. These reduced losses in the tapered SiGe core are attributed to an improvement of the crystalline quality along the fiber length, rather than a change in core size, similar to what was observed following tapering of Si core fibers [16]. Significantly, these loss values are comparable with our first generation tapered polysilicon core fibers [21].

4.2. *Nonlinear absorption*

The nonlinear characterization of the tapered SiGe fiber was initiated with a measurement of the two-photon absorption (TPA) parameter using the setup described in Fig. 3(a), but with the pulsed laser sources as the input pump beam. Measurements of the average output power as a function of coupled input peak power are shown in Fig. 4(a) (coloured circles) for various pump wavelengths ranging from 1.75 μm to 2.35 μm. It can be seen that the output power saturates strongly for wavelengths up to 1.95 μm due to the TPA-induced nonlinear absorption. In general, TPA is strong up to wavelengths ~ 2 μm and then gradually drops to become negligible in the range of 2.2 μm to 3.2 μm, depending on the bandgap of the $Si_{1-x}Ge_x$ alloy [12]. Here the SiGe fiber shows a TPA edge at around 2.35 μm, indicated by the linear trend of the output power in Fig. 4(a). Although three-photon absorption (3PA) is predicted to increase for wavelengths

Optics EXPRESS

beyond the TPA edge [12,22], measurements of the 3PA parameter were not performed in this work due to the limited peak intensity of our pump sources.

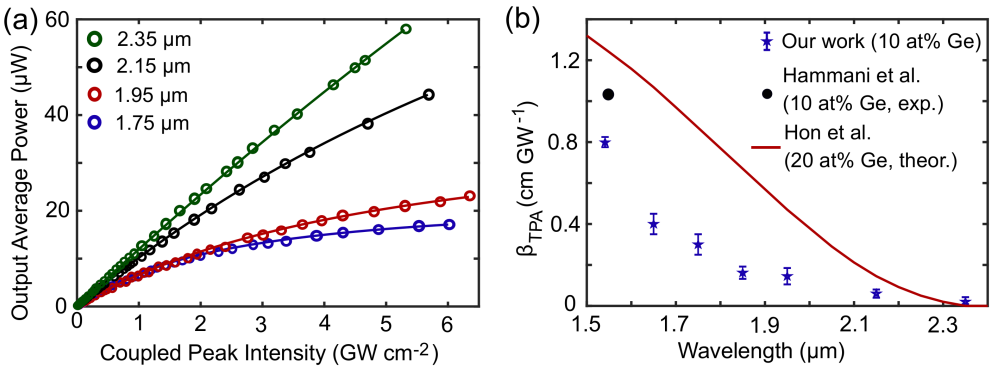

Fig. 4. (a) Nonlinear absorption measurements of the tapered SiGe fiber at different wavelengths. The solid curves are simulated fits to the data (crosses) for the corresponding wavelengths given in the legend. (b) The measured TPA parameter as a function of wavelength extracted from (a), along with experimental TPA data for a planar SiGe waveguide with 10 at% Ge content and theoretical predictions for a 20 at% Ge content material, recreated from [12,23]. Error bars in our experimental data represent the uncertainty in the input powers.

Owing to the micron-sized core of the tapered SiGe fiber, the dispersion length over this wavelength range is much larger than the 6 cm fiber length. Thus it is possible to make use of a simplified nonlinear Schrödinger equation (NLSE) that neglects the role of dispersion and describes the temporal evolution of the intensity profile, from which we can estimate the TPA parameter. This simplified NLSE is coupled to the rate equation for TPA generated free-carriers, with the equations defined as [1]:

$$\frac{dI(z,t)}{dz} = -\alpha_l I(z,t) - \beta_{\mathrm{TPA}} I^2(z,t) - \sigma N_c(z,t) I(z,t), \tag{1}$$

$$\frac{dN_c(z,t)}{dt} = \frac{\beta_{\mathrm{TPA}}}{2h\nu_0} I^2(z,t) - \frac{N_c(z,t)}{\tau_c}. \tag{2}$$

Here $I(z,t)$, α_l, σ, N_c, τ_c represent pulse intensity, linear propagation loss, free-carrier absorption (FCA) coefficient, free-carrier density and carrier lifetime, respectively. These equations were used to fit the experimental data in Fig. 4(a), for all wavelengths (solid lines), to calculate the β_{TPA} values given in Fig. 4(b) (blue stars). Our tapered SiGe fiber exhibits a β_{TPA} value of 0.8 cm GW^{-1} at 1.54 μm, which is comparable to 1.16 cm GW^{-1} estimated at 1.55 μm in a planar SiGe waveguide with same Ge concentration [23]. As expected, the β_{TPA} values decrease for increasing pump wavelengths, finally reaching a value of 0.02 cm GW^{-1} at 2.35 μm, indicating the edge of the TPA window. Comparing these results to the theoretical predictions for a SiGe alloy with 20 at% Ge concentration, as shown by the red curve of Fig. 4(b), we can see that the measured values follow a similar but less steep downward trend, so that the TPA edge is in a comparable position in both cases. This trend is in agreement with the theory for the indirect bandgap calculations for the different alloy materials [12].

4.3. SPM induced spectral evolution

Following the TPA characterization, measurements of the spectral broadening associated with high power pulse propagation in the tapered SiGe fiber were used to estimate the nonlinear Kerr coefficient n_2. The output spectra were measured with an OSA for each pump wavelength

Optics EXPRESS

ranging from 1.54 μm to 2.35 μm at both low and high input peak powers, as shown in Fig. 5. The corresponding coupled intensities for the different peak powers for each pump are given in the legends. We note that the lack of clear SPM induced modulation on the spectra for pump wavelengths above 1.65 μm is due to the fact the the pump pulses produced by the OPO have a significant chirp, which adds noise and bandwidth to spectral shape of the input pulse.

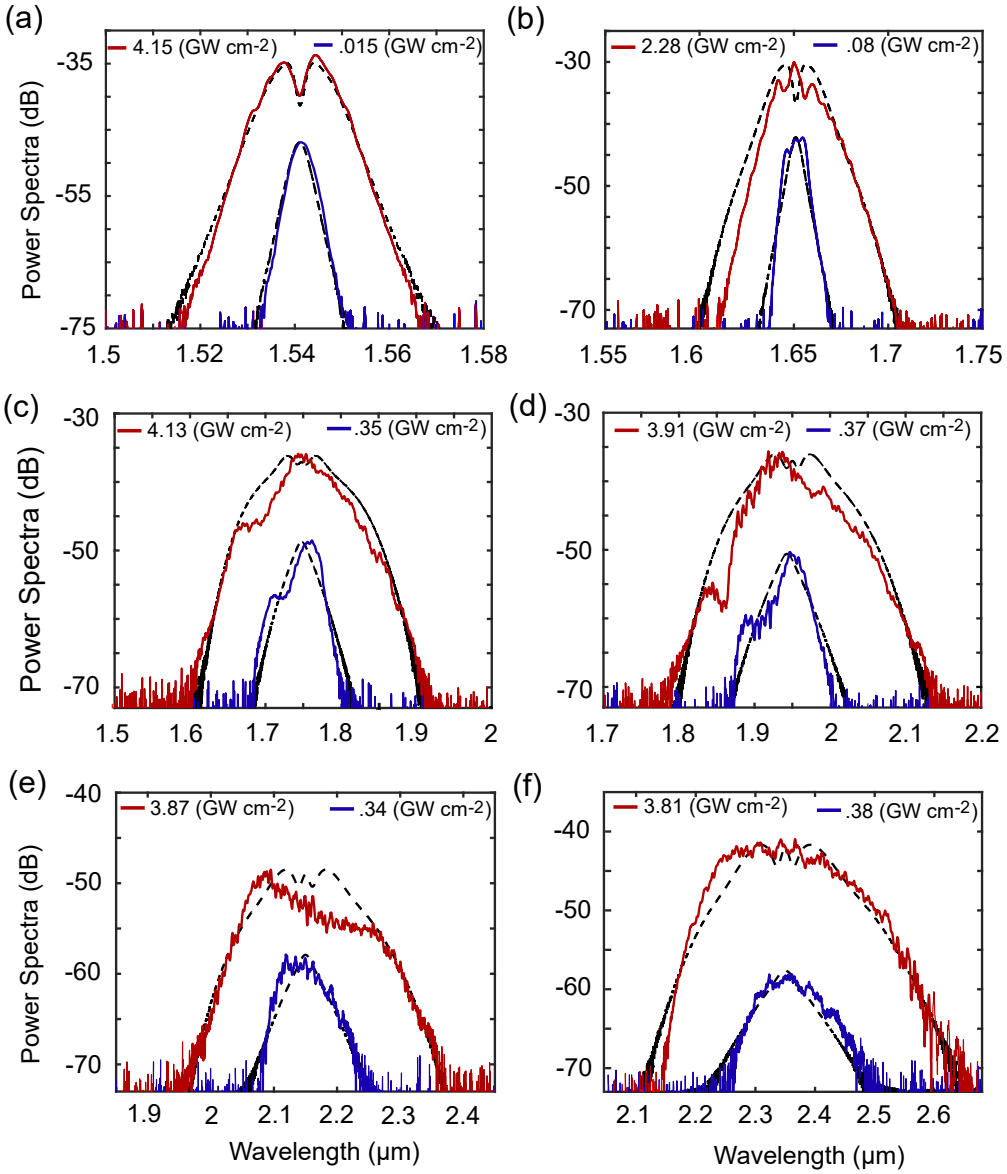

Fig. 5. Experimental power-dependent transmission spectra for pump wavelengths centered at (a) 1.54 μm, (b) 1.65 μm, (c) 1.75 μm, (d) 1.95 μm, (e) 2.15 μm, and (f) 2.35 μm. The dashed lines are numerical fits obtained by solving the generalized NLSE.

Optics EXPRESS

To estimate the n_2 values, the experimental spectra were fitted using the full NLSE equation given by [1]:

$$\frac{dA(z,t)}{dz} = -\frac{i\beta_2}{2}\frac{dA^2(z,t)}{dt^2} + i\gamma|A(z,t)|^2A(z,t) - \frac{1}{2}(\alpha_l + \sigma_f)A(z,t), \tag{3}$$

which is still coupled to Eq. (2) for the generation of the TPA-induced free-carriers. Here, $A(z,t)$, γ, σ_f represent the slowly varying pulse envelope, nonlinear parameter, and the free-carrier contribution, respectively. In this form, the nonlinear parameter is complex, including contributions from both the TPA and Kerr parameter as: $\gamma = i\beta_{\text{TPA}}/2A_{\text{eff}} + k_0 n_2/A_{\text{eff}}$, where A_{eff} is the wavelength dependent effective mode area. Similarly, σ_f is also complex and given by: $\sigma_f = \sigma(1 + i\mu)N_c$, where σ denotes the FCA coefficient defined previously and μ denotes the free-carrier dispersion (FCD). The fitted curves to the measured spectra are displayed as the black dashed curves in Fig. 5, for each pump wavelength. The numerical fits are in good qualitative agreement with the experimental results in terms of the spectral shape and bandwidth, as shown in Table 1 (measured at the −20 dB level). Thus these results indicate the accuracy of the predicted values of n_2 used in the simulations.

Table 1. SPM bandwidth (−20 dB) for different pump wavelengths

Wavelength (nm)	Experimental bandwidth (nm)	Simulated bandwidth (nm)
1541	30	31
1650	58	65
1750	231	237
1950	240	257
2150	368	370
2350	426	427

The obtained n_2 values for each pump wavelength, measured for the 6 cm long tapered SiGe core fiber, are then plotted in Fig. 6(a). It can be seen that n_2 initially increases to a fairly high value of 1.1×10^{-13} cm^2 W^{-1} at 1.75 μm, and then gradually drops to 0.85×10^{-13} cm^2 W^{-1} at 2.35 μm. This trend is as expected from the nonlinear Kramers-Krönig relation linking TPA values to the real part of the third order susceptibility [12]. These n_2 values are also comparable, but slightly higher than our previous estimates of n_2 in polysilicon core fibers over the same wavelength range [21]. It is noted that even higher values of n_2 could be anticipated through increasing the germanium content in SiGe alloy fiber, in line with the predictions in [12].

4.4. Nonlinear figure of merit

The effectiveness of a waveguide for nonlinear processing is often characterized by a nonlinear figure of merit, defined as $\text{FOM}_{\text{NL}} = n_2/(\lambda_0\beta_{\text{TPA}})$, where λ_0 is the pump wavelength. The wavelength dispersion of the FOM_{NL} for the tapered SiGe fiber is shown in Fig. 6(b). This fiber exhibits a FOM_{NL} value of ∼ 0.4 at 1.54 μm, which is slightly higher than our previous reports for the tapered polysilicon core fibers ($\text{FOM}_{\text{NL}} \approx 0.36$) at same pump wavelength [21]. This value is also comparable to previous reports in $Si_{0.9}Ge_{0.1}$ ($\text{FOM}_{\text{NL}} = 0.55$) waveguides [23]. More significantly, however, we observe a steep increase in the FOM_{NL} values for wavelengths above 2 μm, with the FOM_{NL} at 2.15 μm being more than twice as large as the value reported for the polysilicon core fibers. We note that the very large value of the FOM_{NL} at 2.35 μm is limited in accuracy due it being so close to the TPA edge, and 3PA contributions should be considered to truly gauge the nonlinear efficiency. Nevertheless, these results suggest that the SiGe fiber platform should be well suited for nonlinear applications for wavelengths extending beyond the near-infrared.

Optics EXPRESS

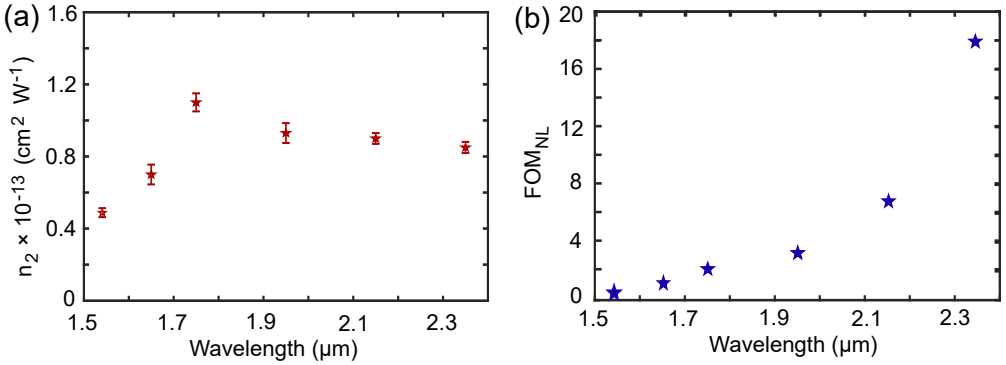

Fig. 6. (a) Wavelength dependence of the Kerr nonlinear coefficient n_2 for the tapered SiGe fiber. Error bars represent the uncertainty in the input pulse peak powers. (b) Wavelength dispersion of the FOM_{NL}.

5. Conclusion

We have experimentally characterized both the linear and nonlinear transmission properties of polycrystalline tapered SiGe core fibers from the telecommunication wavelength band to the mid-infrared spectral region. Material characterization confirmed that our adapted tapering method was able to produce SiGe cores with uniform and high crystalline quality, with optical losses that are much lower than what can be produced directly from the draw tower. Specifically, a tapered SiGe fiber with a core diameter of 3 μm and a length of 6 cm was produced with linear losses of 2.2 dB cm^{-1} at 1.5 μm and 4 dB cm^{-1} at 2.5 μm. Measurements of the nonlinear performance of the SiGe fiber revealed that the nonlinear coefficients are slightly higher than standard Si core fibers, as expected due to the introduction of Ge. The results are also in good qualitative agreement with measurements of planar SiGe alloy waveguides with similar Ge compositions. We expect that continued efforts to optimize the incorporation of different Ge concentrations into the core will allow for the production of a high quality and low loss SiGe core fibers that could be adapted for a wide range of nonlinear applications spanning the near to mid-infrared spectral regions.

Funding. J. E. Sirrine Textile Foundation; Engineering and Physical Sciences Research Council (EP/P000940/1, EP/Y008499/1).

Disclosures. The authors declare no conflicts of interest.

Data availability. Data underlying the results presented in this paper are available in [24].

References

1. P. Mehta, N. Healy, N. F. Baril, *et al.*, "Nonlinear transmission properties of hydrogenated amorphous silicon core optical fibers," Opt. Express **18**(16), 16826–16831 (2010).
2. F. H. Suhailin, L. Shen, N. Healy, *et al.*, "Tapered polysilicon core fibers for nonlinear photonics," Opt. Lett. **41**(7), 1360–1363 (2016).
3. L. Shen, H. Ren, M Huang, *et al.*, "A review of nonlinear applications in silicon optical fibers from telecom wavelengths into the mid-infrared spectral region," Opt. Commun. **463**, 125437 (2020).
4. N. Healy, L. Lagonigro, J. R. Sparks, *et al.*, "Polycrystalline silicon optical fibers with atomically smooth surfaces," Opt. Lett. **36**(13), 2480–2482 (2011).
5. H. Ren, L. Shen, A. F. J. Runge, *et al.*, "Low-loss silicon core fibre platform for mid-infrared nonlinear photonics," Light: Sci. Appl. **8**(1), 105 (2019).
6. D. Wu, L. Shen, H. Ren, *et al.*, "Net optical parametric gain in a submicron silicon core fiber pumped in the telecom band," APL Photonics **4**(8), 086102 (2019).
7. M. Huang, S. Sun, T. S. Saini, *et al.*, "Raman amplification at 2.2 μm in silicon core fibers with prospects for extended mid-infrared source generation," Light: Sci. Appl. **12**(1), 209 (2023).
8. M. Ordu and S. N. Basu, "Recent progress in germanium-core optical fibers for mid-infrared optics," Infrared Phys. Technol. **111**, 103507 (2020).

Optics EXPRESS

9. A. T. Hendrickson, S. C. Aro, J. R. Sparks, *et al.*, "Post-processing ZnSe optical fibers with a micro-chemical vapor transport technique," Opt. Mater. Express **10**(12), 3125–3136 (2020).
10. T. Zaengle, U. J. Gibson, T. W. Hawkins, *et al.*, "A novel route to fibers with incongruent and volatile crystalline semiconductor cores: GaAs," ACS Photonics **9**(3), 1058–1064 (2022).
11. D. A. Coucheron, M. Fokine, N. Patil, *et al.*, "Laser recrystallization and inscription of compositional microstructures in crystalline SiGe-core fibres," Nat. Commun. **7**(1), 13265 (2016).
12. N. K. Hon, R. Soref, and B. Jalali, "The third-order nonlinear optical coefficients of Si, Ge, and $Si_{1-x}Ge_x$ in the midwave and longwave infrared," J. Appl. Phys. **110**(1), 011301 (2011).
13. S. Serna, V. Vakarin, J.-M. Ramirez, *et al.*, "Nonlinear properties of Ge-rich $Si_{1-x}Ge_x$ materials with different Ge concentrations," Sci. Rep. **7**(1), 14692 (2017).
14. L. Carletti, M. Sinobad, P. Ma, *et al.*, "Mid-infrared nonlinear optical response of Si-Ge waveguides with ultra-short optical pulses," Opt. Express **23**(25), 32202 (2015).
15. E. F. Nordstrand, A. N. Dibbs, A. J. Eraker, *et al.*, "Alkaline oxide interface modifiers for silicon fiber production," Opt. Mater. Express **3**(5), 651–657 (2013).
16. Y. Franz, A. F. J. Runge, H. Ren, *et al.*, "Material properties of tapered crystalline silicon core fibers," Opt. Mater. Express **7**(6), 2055–2061 (2017).
17. D. Rouchon, M. Mermoux, F. Bertin, *et al.*, "Germanium content and strain in $Si_{1-x}Ge_x$ alloys characterized by Raman spectroscopy," J. Cryst. Growth **392**, 66–73 (2014).
18. C. D. Salzberg and J. J. Villa, "Infrared refractive indexes of Silicon, germanium and modified selenium glass," J. Opt. Soc. Am. **47**(3), 244–246 (1957).
19. F. Schaffler, "Silicon-Germanium ($Si_{1-x}Ge_x$)," in *Properties of Advanced Semiconductor Materials GaN, AlN, InN, BN, SiC, SiGe*, M. E. Levinshtein, S. L. Rumyantsev, and M. S. Shur, eds. (John Wiley & Sons, Inc., 2001), pp. 149–188.
20. L. Lagonigro, N. Healy, J. R. Sparks, *et al.*, "Low loss silicon fibers for photonics applications," Appl. Phys. Lett. **96**(4), 041105 (2010).
21. H. Ren, L. Shen, D. Wu, *et al.*, "Nonlinear optical properties of polycrystalline silicon core fibers from telecom wavelengths into the mid-infrared spectral region," Opt. Mater. Express **9**(3), 1271–1279 (2019).
22. F. Gholami, S. Zlatanovic, A. Simic, *et al.*, "Third-order nonlinearity in silicon beyond 2350 nm," Appl. Phys. Lett. **99**(8), 081102 (2011).
23. K. Hammani, M. A. Ettabib, A. Bogris, *et al.*, "Optical properties of silicon germanium waveguides at telecommunication wavelengths," Opt. Express **21**(14), 16690 (2013).
24. A. N. Ghosh, M. Huang, T. W. Hawkins, *et al.*, "Dataset for the journal paper titled "Low loss polycrystalline SiGe core fibers for nonlinear photonics"," University of Southampton (2024), https://doi.org/10.5258/SOTON/D2970.